SAND99-0500C
Unclassified
Unrestricted Release

Reprint SMRI
3336 Lone Hill Lane
Encinitas, CA 92024-7262

FRACTURE AND HEALING OF ROCK SALT RELATED TO SALT CAVERNS

by

Darrell E. Munson*, Kwai S. Chan**, and Arlo. F. Fossum*
*Sandia National Laboratories, Albuquerque, NM 87185
**Southwest Research Institute, San Antonio, TX 78228

Prepared for

Spring Meeting
Solution Mining Research Institute
April 14-16, 1999
Las Vegas, Nevada

FRACTURE AND HEALING OF ROCK SALT RELATED TO SALT CAVERNS

Darrell E. Munson*, Kwai S. Chan**, and Arlo. F. Fossum*
*Sandia National Laboratories, Albuquerque, NM 87185[#]
**Southwest Research Institute, San Antonio, TX 78228

ABSTRACT

In recent years, serious investigations of potential extension of the useful life of older caverns or of the use of abandoned caverns for waste disposal have been of interest to the technical community. All of the potential applications depend upon understanding the manner in which older caverns and sealing systems can fail. Such an understanding will require a more detailed knowledge of the fracture of salt than has been necessary to date. Fortunately, the knowledge of the fracture and healing of salt has made significant advances in the last decade, and is in a position to yield meaningful insights to older cavern behavior. In particular, micromechanical mechanisms of fracture and the concept of a fracture mechanism map have been essential guides, as has the utilization of continuum damage mechanics. The Multimechanism Deformation Coupled Fracture (MDCF) model, which is summarized extensively in this work, was developed specifically to treat both the creep and fracture of salt, and was later extended to incorporate the fracture healing process known to occur in rock salt. Fracture in salt is based on the formation and evolution of microfractures, which may take the form of "wing tip" cracks, either in the body or the boundary of the grain. This type of crack deforms under shear to produce a strain, and furthermore, the opening of the wing cracks produce volume strain or dilatancy. In the presence of a confining pressure, microcrack formation may be suppressed, as is often the case for triaxial compression tests or natural underground stress situations. However, if the confining pressure is insufficient to suppress fracture, then the fractures will evolve with time to give the characteristic tertiary creep response. Two first order kinetics processes, closure of cracks and healing of cracks, control the healing process. Significantly, volume strain produced by microfractures may lead to changes in the permeability of the salt, which can become a major concern in cavern sealing and operation. The MDCF model is used in three simulations of field experiments in which indirect measures were obtained of the generation of damage. The results of the simulations help to verify the model and suggest that the model captures the correct fracture behavior of rock salt. The model is used in this work to estimate the generation and location of damage around a cylindrical storage cavern. The results are interesting because stress conditions around the cylindrical cavern do not lead to large amounts of damage. Moreover, the damage is such that general failure can not readily occur, nor does the extent of the damage suggest possible increased permeation when the surrounding salt is impermeable.

#Sandia is a multiprogram laboratory operated by Sandia Corporation, a Lockheed Martin Company, for the U. S. Department of Energy under Contract DE-AC04-94AL5000.

INTRODUCTION

Underground caverns in salt have for many years provided for the storage of liquid and gaseous hydrocarbons and chemical stocks. Over the years, many of these caverns have reached or exceeded their expected life. Older caverns, even those slated for abandonment, represent a potential resource. As a result, in recent years, serious investigations of the potential extension of the useful life of older caverns or the use of abandoned caverns for waste disposal have been of interest to the technical community. However, such investigations are a significant challenge because inevitably the relevant technical issue is determination of the criterion for failure of the cavern or sealing system. Thus, understanding the development of fracture in salt and the conditions of stress and deformation in caverns has become of critical concern. Significantly, the basis for the necessary technology for simulation and prediction of failure in salt has increasingly been the subject of relevant current research. Specifically, knowledge of the fracture and healing of salt has made significant advances in the last decade, and is in a position to give significant insights to older cavern behavior. Clearly, in many situations, especially in waste disposal, safety and environmental concerns will require an ability to predict cavern response well into the future. In this light, we believe it will be of interest to examine quantitative developments in treating the creep, fracture, and healing processes in rock salt, concentrating on a constitutive description that addresses all three of these coupled processes [Chan et al., 1998a].

Naturally, the subject of fracture in solids has historically been of great scientific and technical interest for materials in general, but especially for metals. A number of the concepts useful in the fracture of salt, in fact, have been adapted from knowledge about metals. Over the years, different models have been used to simulate shafts, mine openings, and caverns, usually based on relatively simple material models [Munson and Wawersik, 1991]. Some of the more classic attempts to describe or model all or part of the relevant fracture processes in salt have been based on stress or strain energy, following the same classic developments in metals. Stress based models typically present “flow” surfaces in shear stress and pressure that can represent a number of physical conditions, such as the onset of dilatancy, yielding, or ultimate failure. Such models test the condition of the calculated stress fields against a criterion to determine if the critical condition is exceeded. As formulated, the models are inherently rate-independent. As a consequence, they normally cannot determine critical evolutionary aspects of the fracture process. To overcome this difficulty, some investigators assume damage proportional to the calculated overstress in excess of the stated criterion. Although there are a number of stress based models, the model of Desai and Zhang [1987] represents a typical model formulated on stress. The model used an empirical correlation to estimate permeabilities of salt [Stormont et al., 1992]. Again, many classic stress based models do not treat time-dependent behavior, a behavior thought necessary to accurately model creep and fracture response.

As damage mechanics concepts became more prevalent, the recent models have attempted to use such concepts for application to cavern response. To determine cavern behavior and safety, Lux et al. [1998] utilized a viscoplastic model of creep that incorporated a damage related tertiary creep and failure. Safety was based on decreases in bearing capacity because of time-dependent deformation, along with calculated stress conditions and failure strength determinations. They used an exponential damage growth function. Schulz et al. [1998] used a time power law to obtain the decrease in competence (damage) in order to simulate its’ effect on the cavern roof span and possible cavern collapse with subsequent sink hole development. Cristescu [1993] has proposed a model utilizing a damage parameter based on the energy of microcracking with flow equations incorporating inelastic dilatancy and pressure dependence. In addition the model uses different flow functions for yield, viscoplasticity, and failure. Although this model is capable of describing tertiary creep and fracture, it is not formulated as a typical continuum damage model.

One of the advances in understanding that has produced considerable advantages is the continuum damage mechanics approach, an approach commonly used to treat creep rupture in metals [Hayhurst, 1972; Krajcinovic, 1984]. Often these models originate in an evolutionary equation in the growth of damage based on the isotropic damage variable of Kachanov [1958]. This form of damage variable was used by both Chan et al. [1992, 1998a] and Aubertin et al. [1993, 1998]. Aubertin et al. [1998] used a unified plasticity formulation (SUVIC-D), with backstress as an internal variable, to obtain the transient and steady state creep response, and subsequently an evolutionary development of damage, including tertiary creep and failure. The SUVIC-D model, in a fundamental sense through the backstress, is a stress-based concept. In this respect it differs from the Multimechanism Deformation Coupled Fracture (MDCF) model proposed by Chan et al. [1992, 1998a] which is fundamentally a strain based model, grounded in the mechanisms of dislocation deformation and of microfracture. In this approach the damage is considered as a modifying term on the stressed area and as a direct contributor to inelastic strain rate.

In the work presented here, the complete mathematical development of the MDCF model will be summarized, including the basis for the model. Field experiments and numerical simulations are presented that test the validity of the model and the predictions of the damage field about a salt cavern. The work concludes with a brief summary.

MULTIMECHANISM DEFORMATION COUPLED FRACTURE MODEL

Fundamentally, we know from recent work [Chan et al., 1997a, 1998b] that a comprehensive constitutive model of salt behavior must be able to describe time-dependent transient and steady state creep, evolution of damage producing tertiary creep that results in failure, and healing of damage. Because salt has marked similarities in deformation and fracture to some metals, model formulation has been able to draw upon a broad body of available technical information. In particular, the concept of micromechanical mechanisms of deformation and fracture, especially through the deformation mechanism map [Munson, 1979] and the fracture mechanism map [Ashby, 1983], produces a scientific foundation for the model development. This foundation, combined with utilization of continuum damage, completes the formulation basis. It is essential to note that fracture mechanisms are entirely distinct from plastic deformation mechanisms, even though fracture and deformation may be coupled and their corresponding strains are additive. In contrast to isochoric (constant volume) plastic deformation, non-isochoric fracture processes are highly pressure sensitive. While fracture also normally depends upon the stress direction, here the damage is taken as isotropic. The MDCF model was initially developed specifically to treat the creep and fracture of salt [Chan et al., 1992]. Later necessary developments incorporated nonassociated inelastic fracture flow [Chan et al., 1994] and then extended the model to treat fracture in salt with small impurity inclusions [Chan et al., 1996a]. Recently, a fracture healing process known to occur in rock salt has been incorporated into the model [Chan et al., 1995a]. This model was used to predict the life of a salt structure underground [Chan et al., 1995b]. Thereafter, salt cleavage fracture, although not a time-dependent process, has been addressed [Chan et al., 1996b, 1997b]. These results generated a theoretically complete and data substantiated fracture mechanism map. Developments were based on triaxial compression tertiary laboratory creep testing [Fossum et al., 1993], on healing kinetics studies [Brodsky and Munson, 1994], and on indirect Brazilian tensile creep and cleavage tests [Chan et al., 1997b].

Fracture in salt is based on the formation and evolution of microfractures, which may take the form of “wing tip” cracks, as shown in Figure 1, either in the grain body or at the boundary of the grain, where the principal stresses, σ_1, σ_2, and σ_3, are noted. As this type of crack deforms under shear stress, τ, to produce a strain, opening of the wing cracks may also produce volume strain or dilatancy. These dilatant strains add to the strains of the isochoric creep deformation. The creep

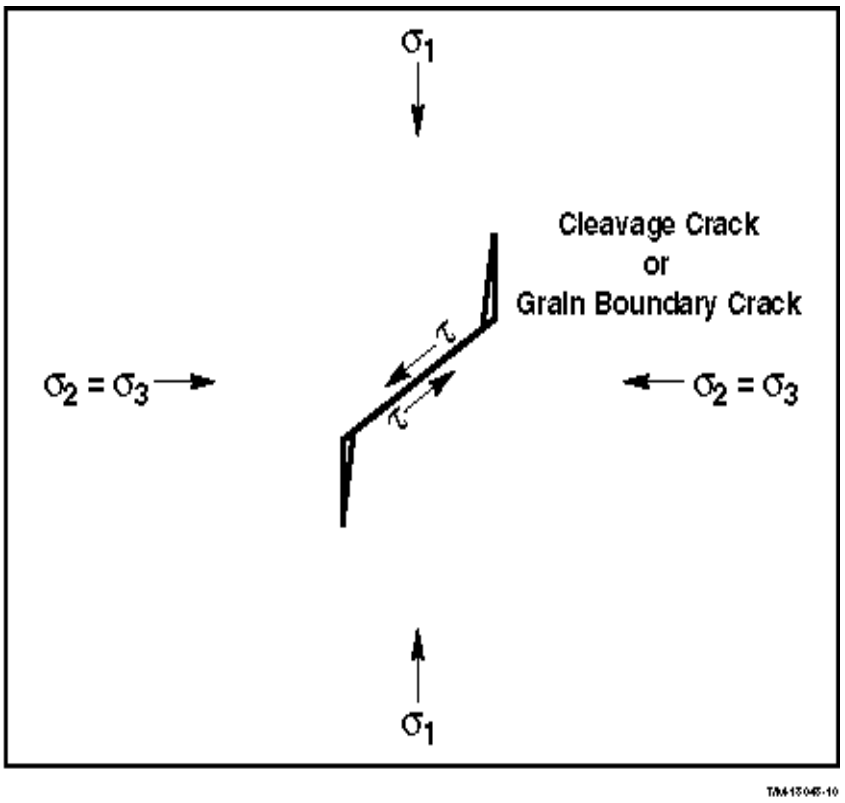

Figure 1. Schematic of Microcrack Development under Stress.

deformation and fracture are coupled because the dilatant strain effectively increases the stress through the Kachanov [1958] effect to increase the creep rate and the creep rate, in turn, directly influences the microfracture evolutionary rate. Under conditions of triaxial compression, which is often the case for natural underground stress situations, the confining pressure may be sufficient to suppress fracture, and deformation will continue indefinitely without failure. However, if the confining pressure is insufficient to suppress fracture, as measured by volume strain, then the fractures will evolve with time to give the characteristic tertiary creep response. Examples of both a fully suppressed (15 MPa) and a tertiary creep curve (1 MPa) are shown in Figure 2. While triaxial compression creep test and constant strain rate conditions may or may not produce tertiary creep and fracture, constant stress rate tests in triaxial compression will always produce stress states in excess of those that suppress fracture and will therefore result in failure. Moreover, when the creep stress condition is tensile, the initial response is creep deformation accompanied by microcrack formation until a critical crack length forms, which then permits cleavage, a separate, time-independent mechanism, to dominate the fracture process. Impurities in the salt may be in the form of small, distinct particles, often as discrete argillaceous (clay) particles. These discrete particle inclusions play an important role in the fracture of salt because they can promote fracture through a change in the local effective stress and pressure conditions. And finally, microfractures, once formed, when again placed under pressure will heal according to relationships based on first order kinetics. The healing of the microfractures is accompanied by an attendant decrease in strain.

In essence, the above description is the fundamental concept behind the mathematical formulation that will be developed throughout the following discussion.

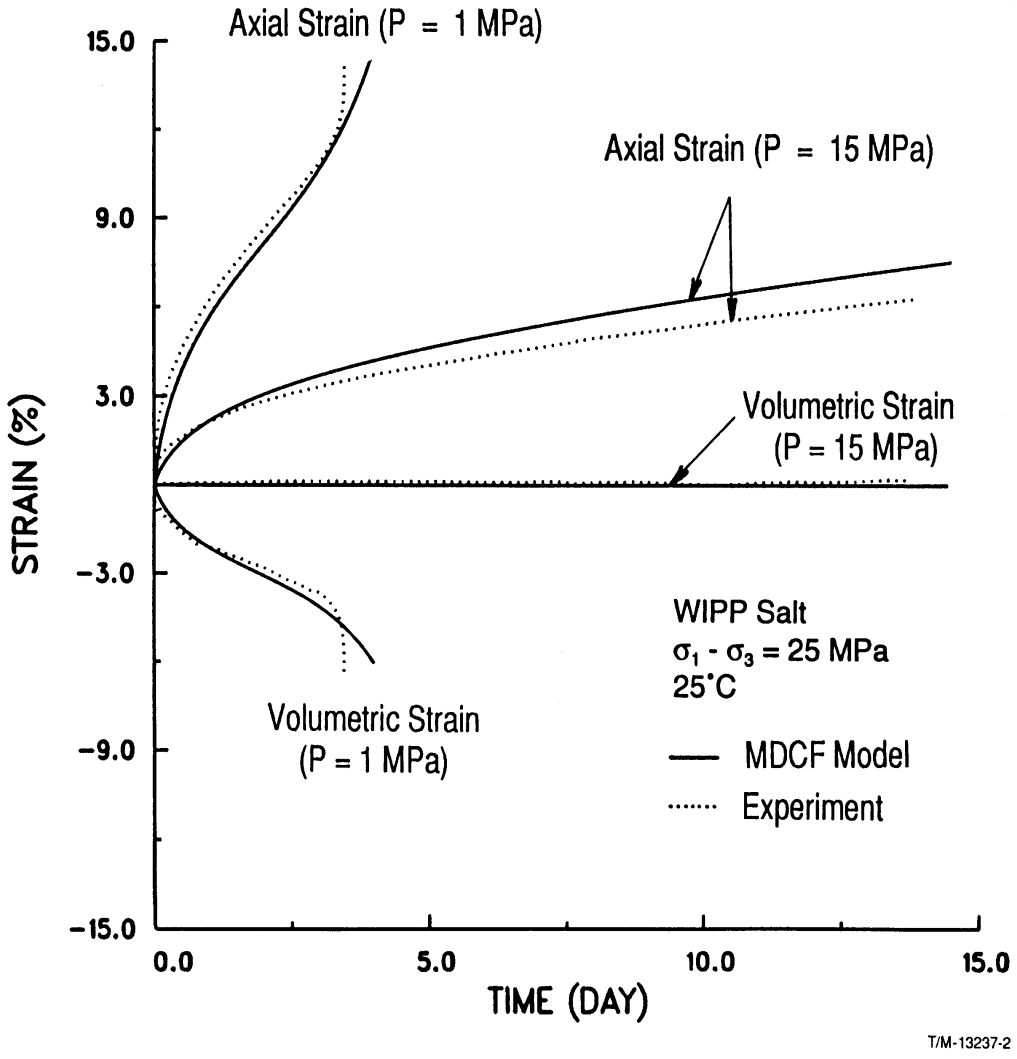

Figure 2. Comparison of MCDF and Experimental Results [after Chan et al., 1997a].

While in this work we are primarily concerned with the inelastic strains, it must be stated that elastic strains are always included in the model. Thus, the total strain is a sum of the elastic and inelastic strains.

Turning now to the inelastic strain, the expression for the inelastic strain rate can be represented as a sum of partial differential equations [Fossum et al., 1988] which according to Chan et al. [1995a] are as follows:

$$\dot{e}^{I}_{ij} = \frac{\partial s^{c}_{eq}}{\partial s_{ij}} \dot{e}^{c}_{eq} + \frac{\partial s^{w_s}_{eq}}{\partial s_{ij}} \dot{e}^{w_s}_{eq} + \frac{\partial s^{w_t}_{eq}}{\partial s_{ij}} \dot{e}^{w_t}_{eq} + \frac{\partial s^{w_h}_{eq}}{\partial s_{ij}} \dot{e}^{w_h}_{eq} \qquad (1)$$

This generalized, coupled inelastic flow equation is stated in terms of the power-conjugate equivalent stress measures, s^{i}_{eq}, and equivalent strain measures, e^{i}_{eq}. Here, as the terms

indicate, the indices denote the i^{th} process for creep (c), shear damage (ω_s), tensile damage (ω_t), and healing (h), respectively. The superimposed (°) indicates the differential with respect to time. Each of the processes on the right hand side of the equation contain a conjugate stress measure (or flow law) and a conjugate strain rate measure (or kinetic equation) for the individual contributions to the flow, as formulated separately in the following sections.

CREEP FORMULATION

Munson and Dawson [1984] and Munson et al. [1989] initially developed the Multimechanism Deformation (M-D) creep model. It is this model that later formed the basis of the MDCF model. The kinetic equation, or strain rate measure, results from three dislocation mechanisms identified on the dislocation mechanism map as relevant to the stress conditions for caverns. The steady state rate is given as the sum of the individual mechanism rates [Munson and Dawson, 1984]:

$$\dot{e}_s = \sum_{i=1}^{3} \dot{e}_{s_i} \qquad 2$$

where the subscripts here denote the i^{th} mechanism. The mechanisms are (1) dislocation climb controlled creep, (2) an empirically well defined, but unknown mechanism, and (3) dislocation glide controlled creep, respectively. Steady state creep rates for these three mechanisms are

$$\dot{e}_{s_1} = A_1 e^{\frac{-Q_1}{RT}} \left(\frac{s_{eq}}{m(1-w)} \right)^{n_1}$$

$$\dot{e}_{s_2} = A_2 e^{\frac{-Q_2}{RT}} \left(\frac{s_{eq}}{m(1-w)} \right)^{n_2}$$

$$\dot{e}_{s_3} = \left| H\left(s_{eq} - s_0\right) \right| \left(B_1 e^{\frac{-Q_1}{RT}} + B_2 e^{\frac{-Q_2}{RT}} \right) \sinh\left[\frac{q\left(\frac{s_{eq}}{1-w} - s_0 \right)}{m} \right]$$

where the A's and B's are structure factor constants, Q's are activation energies, T is the absolute temperature, R the universal gas constant, μ the shear modulus, n's are the stress exponents, q is the stress constant, H is the Heaviside function with the argument ($\sigma_{eq} - \sigma_0$), and σ_0 is the stress limit of the dislocation glide mechanism. The damage parameter, ω, is a scalar measure of isotropic damage [Kachanov, 1958].

These equations differ from those originally developed for the M-D model by the inclusion of the damage parameter. The damage has the effect of decreasing the area over which the force is

applied, thereby increasing the effective stress (not the applied stress, which remains constant) and hence the creep rate. Obviously, the damage parameter appears in this form only in those equations where it is appropriate, as will be apparent.

Total creep rate is obtained through a transient creep multiplier, F, that acts on the steady state rate as given in the function

$$\dot{e}_{eq} = F\,\dot{e}_{s} \tag{4}$$

In terms of dislocation concepts the transient response reflects changes in internal defect structure. The potentials from the internal defect concentrations drive the transient creep process. As a result, the transient function, F, contains three branches, consisting of a workhardening branch, a steady state branch, and a recovery branch, respectively, as follows:

$$F = \begin{cases} e^{\Delta\left(\left(\frac{z}{1-\frac{z}{e_t^*}}\right)^2\right)} & ;\ z < e_t^* \\ 1 & ;\ z = e_t^* \\ e^{-d\left(\left(\frac{z}{1-\frac{z}{e_t^*}}\right)^2\right)} & ;\ z > e_t^* \end{cases} \tag{5}$$

Here, Δ and δ are the workhardening and recovery parameters and ζ is the isotropic transient strain state parameter. Workhardening and recovery parameters are functions of stress

$$\begin{aligned} \Delta &= a_w + b_w \log\left(\frac{s_{eq}}{m(1-w)}\right) \\ d &= a_r + b_r \log\left(\frac{s_{eq}}{m(1-w)}\right) \end{aligned} \tag{6}$$

where the α's and β's are constants; however, under most typical cavern loading situations the δ may be approximated as a constant. The transient strain limit, ε^*_t, is given by

$$e_t^* = K_0 e^{cT}\left(\frac{s_{eq}}{m(1-w)}\right)^m \tag{7}$$

where K_0, c, and m are constants. The evolutionary rate of the isotropic transient strain state parameter is governed by

$$\dot{z} = (F - 1)\dot{e}_s \qquad 8$$

As is apparent, the evolutionary rate of the transient strain state parameter must become zero during steady state creep.

The conjugate equivalent stress measure or flow law that applies to the creep process in Eq. 1 is

$$s^{c}_{eq} = \left| s_1 - s_3 \right| \qquad 9$$

which is the Tresca maximum shear stress criterion. This criterion has been shown experimentally from multiaxial, hollow cylinder tests on salt to be preferred over other criteria [Munson et al., 1989]. Furthermore, numerical simulations of underground room closures at the Waste Isolation Pilot Plant (WIPP) facility confirm this model, as well as this criterion [Munson, 1997].

FRACTURE FORMULATION

The kinetic, conjugate strain rate equations for shear and tensile, damage-induced inelastic flow are developed from a concept that microfractures can undergo shear deformation and that wing-tip cracks can occur as part of these microfractures, as shown in Figure 1. It is thought the cracks occur at the ends of dislocation slip bands and, as a result, the form of the kinetic equation is the same form as that previously developed for dislocation glide. Thus, from Chan et al. [1988a]:

$$\dot{e}^{wi}_{eq} = F^{wi}\dot{e}^{wi}_{s} \qquad 10$$

where "*i*" indicates either the shear or the tensile damage component and $F^{\omega i}$ is a transient function for the respective mode of damage. The transient function for damage is given by

$$F^{wi} = F\ \exp\left[\frac{c_4\left(s^{wi}_{eq} - c_5\right)}{c_7}\right] \qquad 11$$

where c_4, c_5, and χ_7 are constants. Fracture and creep are clearly coupled because F is the transient function from the creep deformation formulation. Then, the kinetic equations for damage induced flow during steady state creep are expressed as

$$\dot{e}^{wi}_{s} = c_0\left(\sum_{k=1}^{2} B_k e^{\frac{-Q_k}{RT}}\right) w_0 e^{c_3 w}\left[\sinh\left(\frac{c_2 s^{wi}_{eq} H\left(s^{wi}_{eq}\right)}{m\left(1 - w\right)}\right)\right]^{n3} \qquad 12$$

where c_0, c_2, c_3, and n3 are constants, and ω_0 is the initial value of the damage variable, ω. The structure factors are summed over the *k* indices on B and Q.

The damage evolution equation is of the form

$$\dot{w} = \frac{c_4}{t_0} w \left[\ln\left(\frac{1}{w}\right) \right]^{\frac{c_4+1}{c_4}} \left\{ \left[\frac{s_{eq}^{w_s} H\left(s_{eq}^{w_s}\right)}{c_s} \right]^{c_{3s}} + \left[\frac{s_{eq}^{w_t} H\left(s_{eq}^{w_t}\right)}{c_t} \right]^{c_{3t}} \right\} \quad 13$$

where χ_4, χ_s, χ_t, χ_{3s}, and χ_{3t} are constants; t_0 is a reference time.

As initially noted, damage in compression is considered to arise from shear sliding of microcracks and by opening of the wing-tip cleavage cracks that can develop on the shear cracks. As a consequence, the resulting inelastic flow includes deviatoric and dilational components. Normally, each of these components would require an individual stress measure for use in Eq.1. We will in fact define these two stress measures for the flow. However, unlike the creep deformation, the fracture strain is nonassociated [Chan et al., 1994] and therefore requires the use of two conjugate stress measures in Eq. 1 for the shear component. To differentiate between these two measures, the flow stress measure will have a subscript *f*, while the kinetic equation will have a subscript *k*. Different stress measures were found necessary to adequately represent the experimental data, a situation that is not uncommon. As specified later, the healing process is also known to be nonassociative.

Thus, according to the previous discussion, the conjugate stress measure or flow law of Eq.1 for the shear component of fracture is given by

$$s_{eq}^{w} \Big|_f^s = \left| s_1 - s_3 \right| - \frac{c_2 c_8}{3} \left[I_1 - s_1 \right] \quad 14a$$

and the comparable nonassociated, conjugate stress measure for use in the kinetic equation, Eq. 11, for the shear component of fracture is

and the conjugate stress measure for use in flow law and the kinetic equation for the tensile component is given by the following:

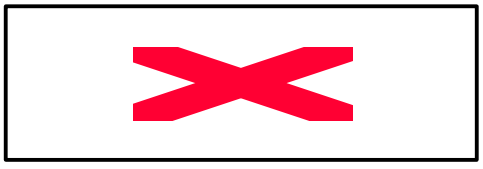

here, χ_1, χ_2, χ_6, χ_7, and χ_8 are constants and f_p is a parameter related to volume and effectiveness of the impurity content.

In Figure 3 two creep curves are shown, one is obtained in triaxial compression, whereas, the other is in indirect tension. While each curve has the features of a typical creep curve with an initial decreasing-rate transient response, a brief steady state response, and tertiary response, the strain magnitudes are considerably different. The tensile behavior suggests a ductile but very weak material, with relatively small strains to failure. In tension the ductile behavior soon terminates in a cleavage fracture. This occurs as soon as one of the microcracks grows large enough to exceed the critical size-stress criteria for cleavage. Cleavage is a rate-independent process. Although the cleavage mechanism is one of the important mechanisms of the mechanism map, we will not discuss it further here.

The pressure dependence of fracture is contained in Eq. 14b, where the second term on the right hand side of the equation is essentially a pressure term that diminishes the magnitude of the equivalent conjugate stress as pressure increases. The shear stress ($J_2^{1/2}$)-pressure (I_1) invariant relationship is shown in Figure 4 for clean salt. The curve shown is the boundary along which the damage rate is zero. Damage evolves for all stress states above and to the left of the curve; while damage is suppressed for all stress states below and to the right of the curve. Healing of previously damaged salt can take place only for stress states within the region below and to the right of the curve, which is the region of damage suppression.

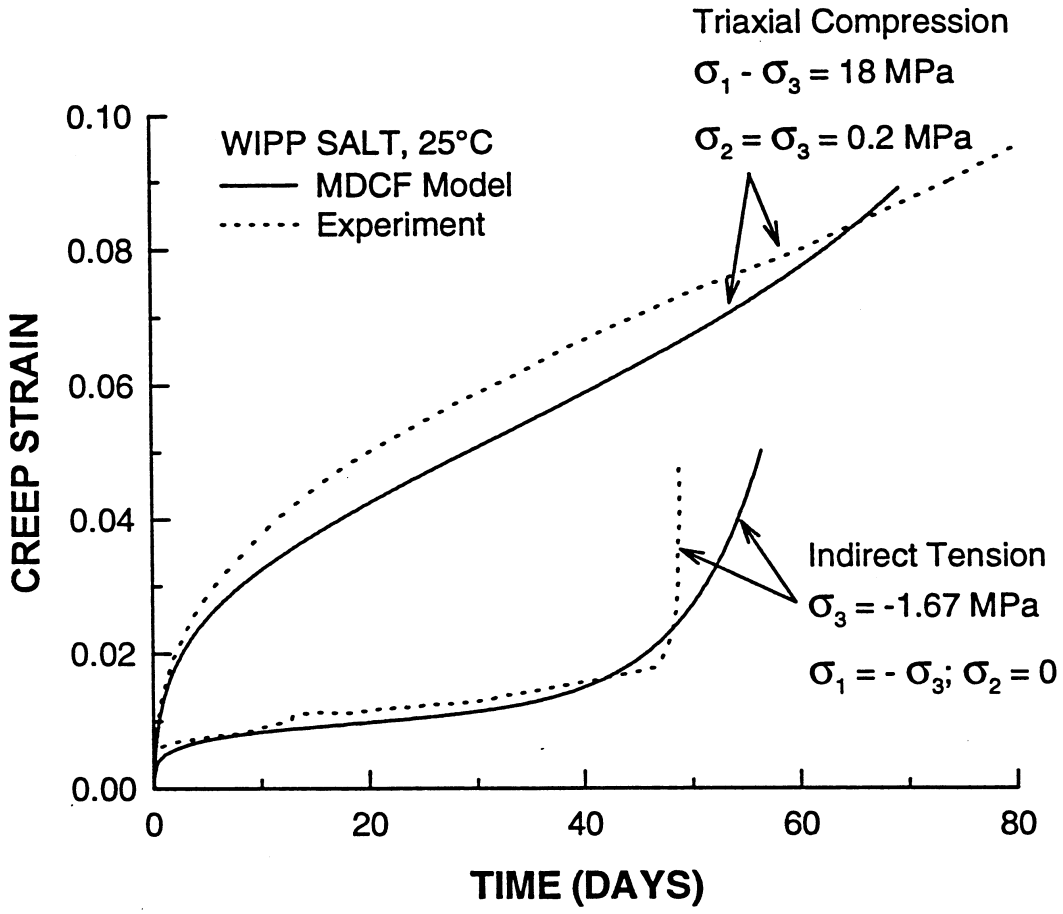

Figure 3. Comparison of Triaxial Compression and Indirect Tension Curves [Chan et al., 1997b].

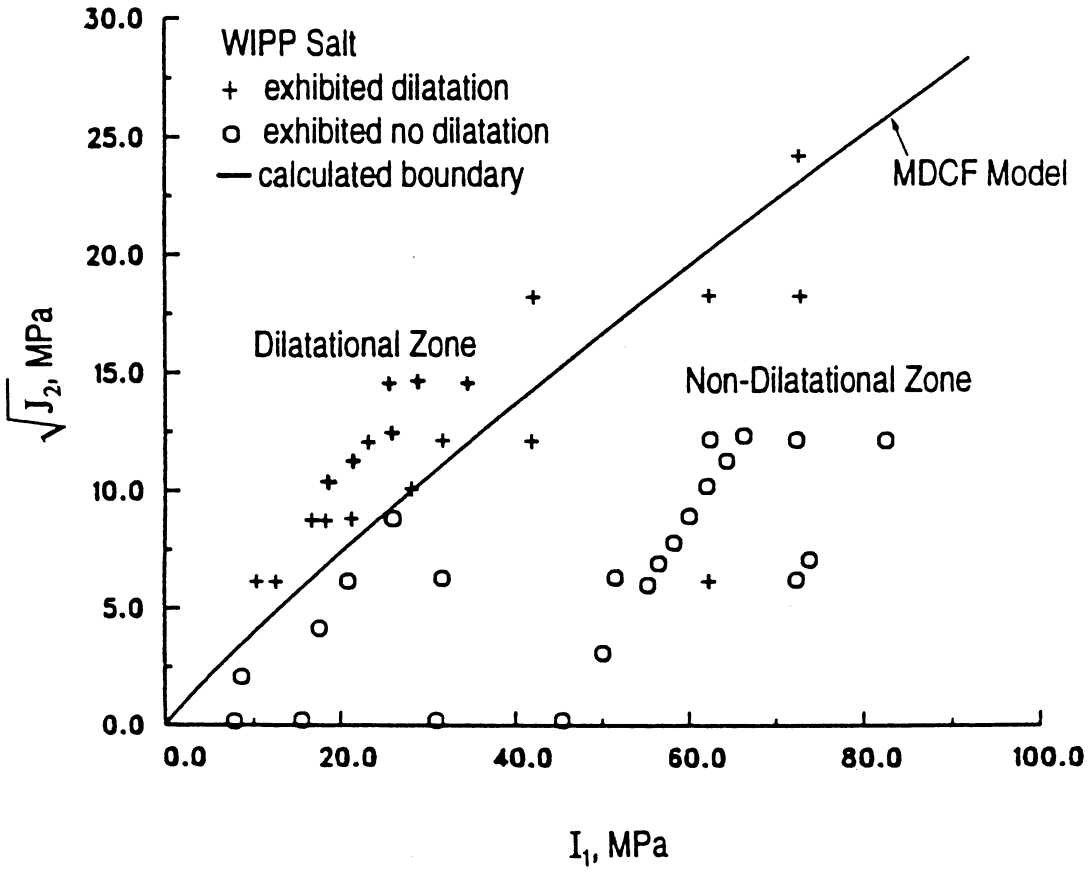

Figure 4. Damage Evolution Zero Rate Curve for Clean Salt [Chan et al., 1997a]

Impurities that form particles in salt can have a rather significant effect on the fracture behavior. The particle alters the local stress field around the particle to decrease the effective confining pressure which in turn, through the pressure term of Eq. 14b, permits microfractures to form more readily [Chan et al., 1996a]. This is accounted for in the equation through the f_p parameter, which is given by

$$f_p \cong 1 - p_1 r \qquad 15$$

where p_1 is a constant and ρ is the volume fraction of the impurity particles. Other types of second phase impurities, not in the form of particles, would probably not have the same effect. The effect of particles on the zero damage curve of Figure 4 is to displace the curve to lower shear stress ($J_2^{1/2}$) values as the particle content increases. Actually, various impurity levels produce a family of damage boundary curves progressing downward from the curve shown in the figure.

HEALING FORMULATION

Healing of fractures is a process distinctively related to salt. Experimental investigation of the healing in initially damaged salt specimens [Brodsky and Munson, 1994] indicated first-order kinetic processes for both crack closure and crack healing, the latter is perhaps somewhat related

to sintering. However, after careful analysis, the healing rate function was taken [Chan et al., 1995a] as a simplified functional form with a single characteristic time, as follows:

$$h = \frac{w\left(s_{eq}^{h} - s_{b}\right) H\left(s_{eq}^{h} - s_{b}\right)}{tm} \qquad 16$$

where

$$s_{b} = c_{7} \left| \frac{s_{1} - s_{3}}{c_{2} c_{7}} \right|^{\frac{1}{c_{6}}} \qquad 17$$

The nonassociated equivalent conjugate stress measures for use in Eq. 1 and Eq. 16 is given by

$$s_{eq}^{h} = \frac{1}{3}\left(I_{1} - c_{10} s_{1}\right) \qquad 18$$

where χ_{10} is a constant with different values for the flow equation and the kinetic equation.

At this point we have developed all of the kinetic functions, or conjugate strain rate measures, together with the appropriate flow potentials, or conjugate stress measures, for creep, fracture, and healing. Although the MDCF model we have developed is quite complicated, its agreement to experiment as indicated in previous figures suggests it is also quite accurate. Because it is thought to be a rather rare condition in the underground, the cleavage fracture condition will not be discussed here. Further details on cleavage are given in Chan et al. [1997b]. In addition, Chan et al. [1998a] gives a fracture mechanism map in terms of mechanism fields in stress space that clearly indicates the relationship of the relevant processes.

CONFIRMATORY SIMULATIONS OF FIELD DATA

Perhaps one of most difficult problems is to identify and measure dilatant behavior of salt in the field. Even though the final condition, failure, is one of the most easily observed phenomena, the microcracks that are the precursor to total failure are completely hidden from visual detection. Nevertheless, there have been at least two field tests where the dilatant damage could be detected indirectly. One test observed the difference in ultrasonic wave speeds with depth into the salt around a shaft, as a measure of the change in elastic modulus because of dilatancy. The second observed the drainage of included brine from the salt around a circular tunnel. This was taken as a measure of the evolution of dilatant damage in the salt. Both of these situations were analyzed using the MDCF model of creep and fracture.

In an additional simulation, the accumulation of damage around an underground room in salt was compared to a final failure condition. In this case, it was necessary to trace the locations of the maximum damage contours around the room and correlate these locations to the configuration of the final slab formation. The calculated roof failure times were compared to the actual times.

In these calculations, a uniform set of creep and fracture parameter values was used, as given in Table I, while the temperature dependent healing parameters are given by Chan et al. [1998b].

Table I. Material Parameters for Creep and Fracture of WIPP Salt [composite Chan et al., 1997a and Munson, 1997].

Elastic Properties

μ	12.4 GPa	E	31.0 GPa	ν	0.25

Creep and Fracture Properties

	M-D Creep Constants		MDCF Damage Constants
	Clean	Argillaceous	Clean and Argillaceous
A_1 (sec^{-1})	8.386 E22	1.407 E23	$\chi_1 = 6$
Q_1 (J/mol)	1.045 E5	1.045 E5	$\chi_2 = 9$
n_1	5.5	5.5	$\chi_{3s} = 5.5$
B_1 (sec^{-1})	6.086 E6	8.998 E6	$\chi_{3t} = 40$
			$\chi_4 = 3$
A_2 (sec^{-1})	9.672 E12	1.314 E13	$\chi_s = 231.0$ MPa
Q_2 (J/mol)	4.180 E4	4.180 E4	for $\sigma > \sigma_0$
n_2	5.0	5.0	$\chi_s = 351.1$ MPa
B_2 (sec-1)	3.034 E-2	4.289 E-2	for $\sigma < \sigma_0$
			$\chi_t = 15.15$ MPa
σ_0 (MPa)	20.57	20.57	$\chi_6 = 0.75$
q	5.335 E3	5.335 E3	$\chi_7 = 1$ MPa
			$\chi_8 = 0.1$
K_0	6.275 E5	6.275 E5	$c_0 = 5$ E4
m	3.0	3.0	$c_2 = 850$
c (K^{-1})	0.009198	0.009198	$c_3 = 10$
			$c_4 = 6$
α_w	-17.37	-14.96	$c_5 = 25$ MPa
β_w	-7.738	-7.738	$t_0 = 1$ sec
δ (replaces α_r and β_r)	0.58	0.58	$n_3 = 3$
			$\omega_0 = 1$ E-4
R (J/mol ^oK)	8.3143	8.3143	$p_1 = 20.6$ for argillaceous only

ULTRASONICS IN SALT AROUND A SHAFT

At the WIPP facility, an opportunity existed to instrument the salt adjacent to a new shaft with ultrasonic wave speed detectors [Munson et al., 1995]. The measurement station was at a depth of 626 m in a 6.2 m diameter shaft. Three 15.6 m deep holes were drilled at an angle of 45^o into the shaft wall. The holes were separated by 1.5 m. Some 40 transducers placed in the holes permitted the ultrasonic wave velocities to be determined in three orthogonal directions: tangential, axial and radial. The measured change in ultrasonic velocity was related to the change in elastic modulus caused by the microcrack dilatancy induced by the salt creep. Interpretation of the change in wave speeds requires a complicated conversion between the wave speed and dilatancy because the MDCF calculated quantities and the measured quantities are only indirectly related. The MDCF model simulated the shaft geometry to calculate the amount of volume strain or damage during the time since excavation. Then, independently, measurements were made of the ultrasonic wave

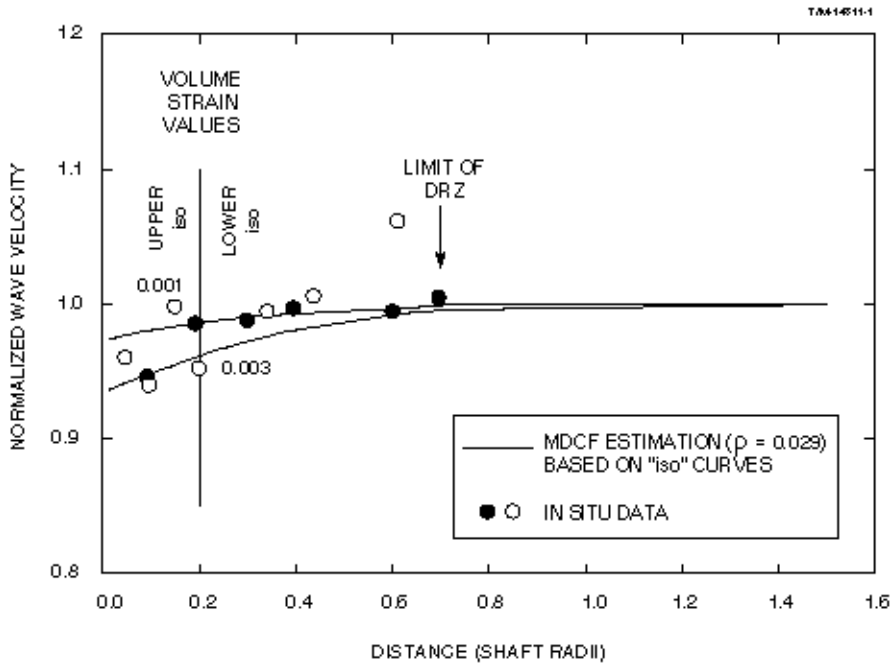

Figure 5. Calculated and Measured Ultrasonic Velocity and Damage [after Munson et al., 1995].

speed as a function of dilatancy in a laboratory specimen strained in triaxial compression. Dilatant strain occurs in both the radial and axial directions. It was necessary to convert these directional dilatancy values into a volume strain in order to compare the laboratory quantities to the model calculation. In Figure 5, the range of the laboratory uncertainty is noted by the two calculated curves, one at a normalized strain limit of 0.001 and the other at 0.003. Even with some uncertainty in the laboratory measurements, the agreement between the field measurements and calculations, as shown in the figure, is reasonable

BRINE RELEASE AROUND A CIRCULAR TUNNEL

In order to address the possible seepage of brine with time into the WIPP from the surrounding salt, a large-scale experiment was fielded at the facility depth of about 655 m. The experiment was conducted in a 2.90 m diameter by 108.6 m long cylindrical, horizontal, blind-ended excavation made by a tunnel boring machine. The tunnel was sealed at the open end to prevent loss of moisture. Over a period of nearly six years, the amount of brine seepage was measured, as shown in Figure 6. The accumulation had to be corrected for an early nearly two year, unsealed period where evaporation to the mine ventilation occurred, and a final one-year period where the seal was circumvented by fractures. During both of these periods essentially no brine accumulation could be measured. Initially, the analysis of brine inflow was based on hydrologic flow in the salt. Although, hydrologists, with some difficulties, calculated the Darcy flow based on an assumed far field permeability [Webb, 1992], there was an alternative, and equally plausible, explanation of the observed behavior. Munson et al. [1996] proposed a model based on damage accumulation around the excavation that progressively released and drained the approximately 1.0% of entrapped brine. In the model brine release is regulated by the amount of damage and by the volume of salt swept by the damage front. The result of this analysis is shown in the figure, with quite acceptable agreement. The damage field calculated by the MDCF model at 10 years is shown in Figure 7, including the differences caused by a horizontal interbed (clay and anhydrite) seam that intersects the room.

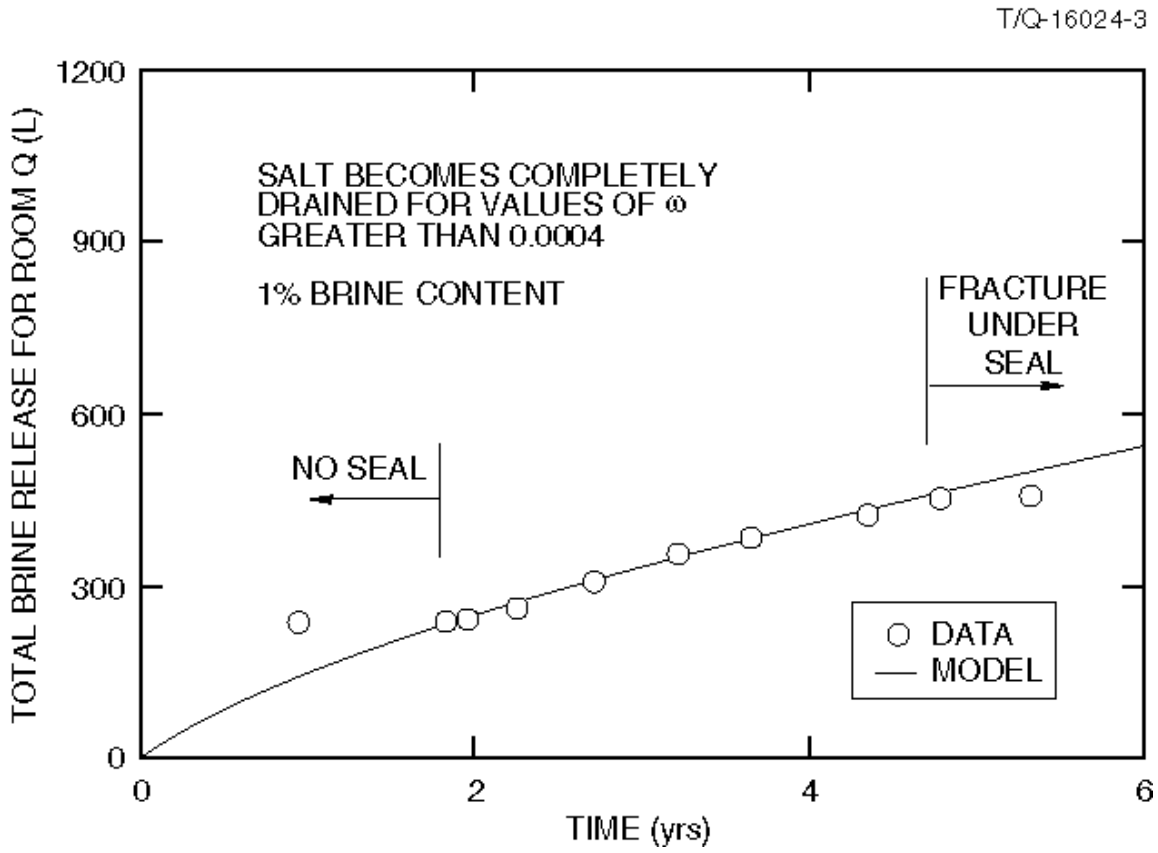

Figure 6. Measured and Calculated Damage Release of Brine [after Munson et al., 1996].

FAILURE AROUND AN UNDERGROUND ROOM IN SALT

The MDCF model permits calculation of the life expectancy of a room [Chan et al., 1995b] by taking the practical limit of damage at failure to be about 0.15. At this level of damage, laboratory observations indicate the salt no longer has integrity. There were a series of four test rooms at the WIPP that were excavated early in the project. The rooms were at the storage horizon of 655 m and had dimensions of 3.96 m height by 10.06 m width, and 91.44 m length. The rooms were separated by 30.48 m thick pillars. Borns and Stormont [1989] documented physical observations of the massive failures. Observable fracture in the rooms occurred in the floor and roof, with indirect indications of slabbing fractures in the ribs. Loss of rib integrity was determined by essentially unconstrained flow from pressurized boreholes through the subparallel fractures. Floor fractures caused scalloped shaped fractures. These fractures began with thin edges near the rib-floor junction and continued downward into the floor to penetrate until they intersected at about quarter room span a massive anhydrite layer about 1.0 m beneath the floor. Floor fractures were verified by visual surface observations and by large diameter core holes drilled into the floor. Eventually, the roof of the room fell to reveal a massive inverted, shallow bowl shaped slab, thin at the edges near the intersection of the room ribs and roof and thick at the middle at the room center. The damage around a room was calculated using an approximation of an infinite series of rooms with symmetry planes at mid-room span and mid-pillar thickness [Chan et al., 1995b]. Results at 10 years of the MDCF calculation through a room cross-section are shown in Figure 8. As is apparent, the concentration of damage occurs in the floor in the scalloped configuration consistent with the observed eventual fractures. The ribs also show the damage consistent with the formation

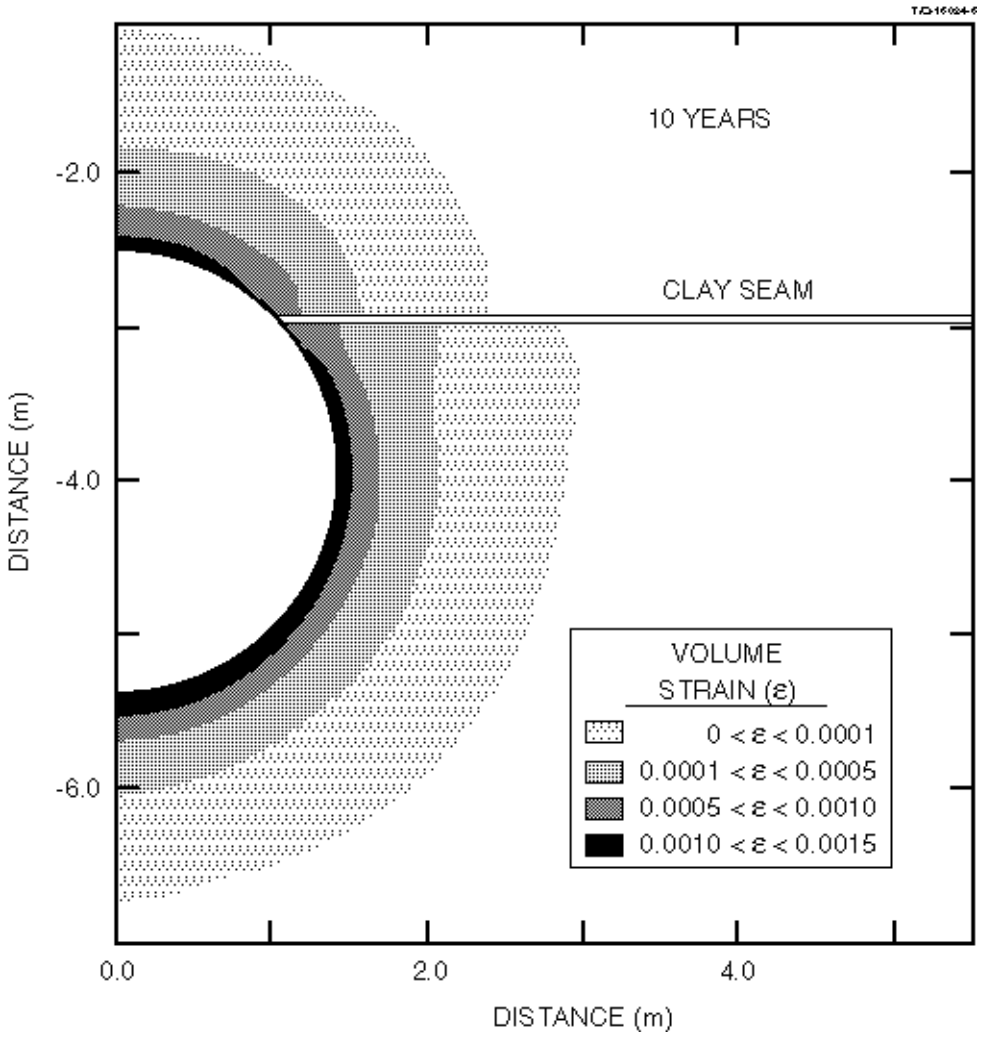

Figure 7. Calculated Damage Contours around Tunnel at 10 Years [after Munson et al., 1996]

of lenticular slabs. And, further, the damage accumulation in the roof shows an arc shaped configuration, with greater concentrations of damage at the roof corners, consistent with the shape development of the final roof spall. From the calculations, life expectancy, or time for roof fall, was about 10 years. Indeed, the roof fall occurred in one room at 8 years and in another room at 11 years. The remaining two rooms, although sealed so no observations were possible, had not yet failed at the time of the second roof fall. A life expectancy calculation of this type is quite demanding because the prediction of long-term response must contend with the inherent time uncertainty in the final loss of integrity. Small differences in actual damage evolution occur in the real world for a number of reasons, possibly because of slightly different impurity contents or of local bedding geometries. All of which can cause a significant difference in the time to failure. Nevertheless, few, if any, models prior to this time have been sophisticated enough to calculate the life expectancy of underground rooms, as we have presented here.

SIMULATIONS OF CAVERN DAMAGE

Even though the evidence is indirect, it appears that the MDCF model calculates damage and fracture in a fundamentally correct manner with some assurance. As a result, we want to apply the

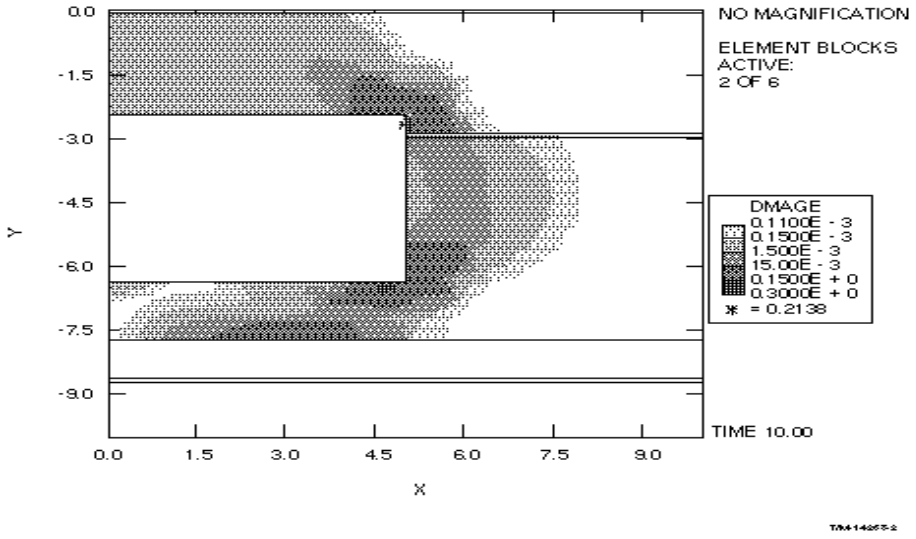

Figure 8. Damage Contours around a WIPP Room [Chan et al., 1995b].

model to the behavior of storage caverns, primarily to postulate interior cavern conditions where the possibility of visual observation is severely limited. The simplest calculation is one presented initially in a study of interior cavern conditions relative to creation of salt falls [Munson et al., 1998]. The specific salt caverns of the study were those of the Strategic Petroleum Reserve (SPR) sited in several salt domes of the Gulf Coast. The calculational mesh was a "pineapple slice" confined with the formation stress appropriate for the given depth applied both top and bottom. This is equivalent to axisymmetric situation modeling the radial creep and damage behavior of a cylindrical shaft or cavern. In the calculation, the impurity content was assumed to be about 3.0%, equivalent to the argillaceous halite of the WIPP. The stress differential between the cavern interior and the surrounding salt was 14.7 MPa. While the stress differential is the correct measure of the driving stress for creep and fracture, most people think of overburden and fluid depths or pressures. The fluid pressures can of course vary with fluid type (gas for instance) and operation practice. For the SPR caverns, the differential stress is the difference between the lithostatic (overburden) pressure and the internal fluid pressure (including the operating pressurization). As a result, a differential stress of 14.7 MPa occurs near the cavern bottom and this is where the maximum damage would be expected. Physically, the caverns are about 60 m in diameter by

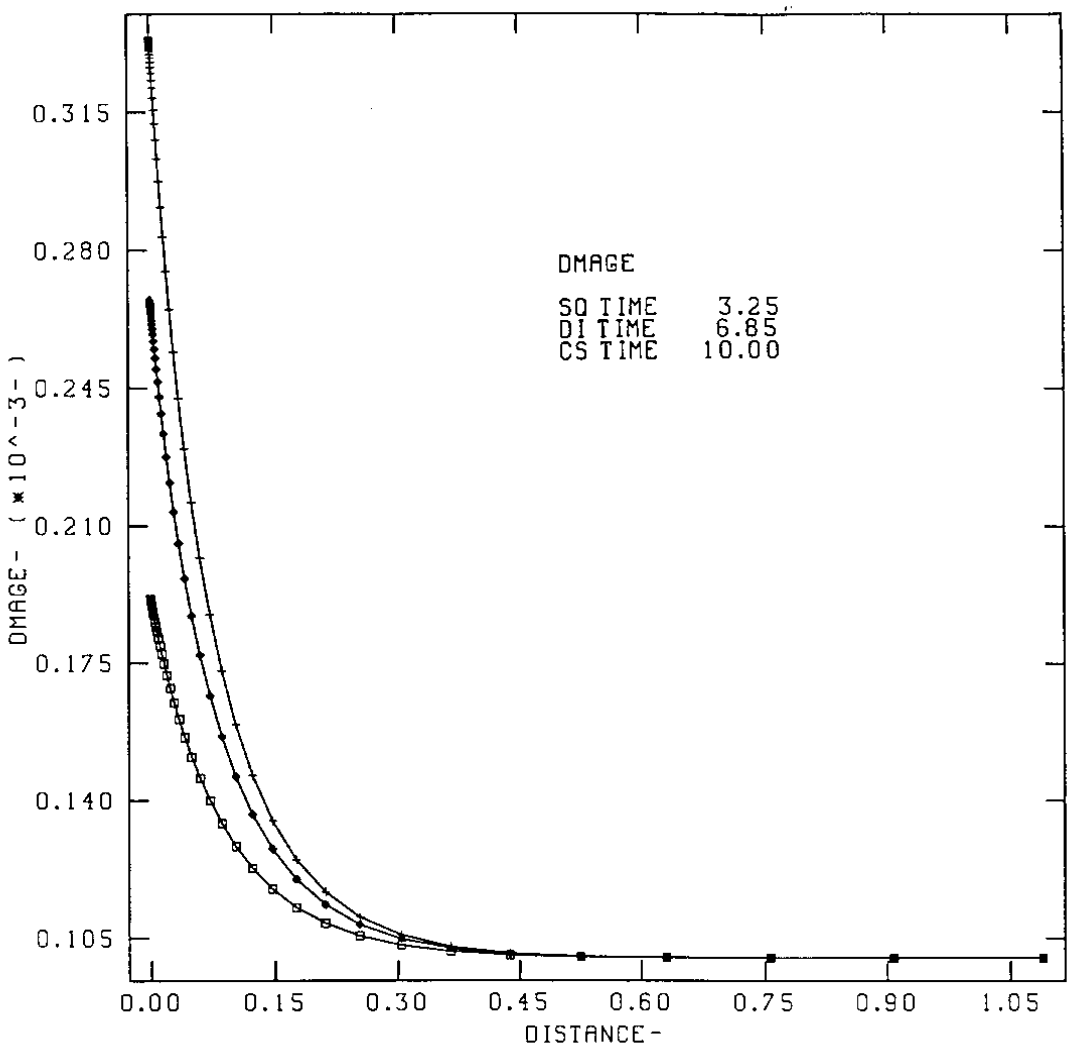

Figure 9. Cylindrical Cavern Damage for 14.7 MPa Stress Differential [after Munson et al., 1998].

about 600 m high and are situated beneath an overburden depth of about 600 m. The overburden is near-surface earth, cap rock, and salt, in that order with depth. The caverns store crude oil, normally under slightly pressurized conditions. In these caverns, the damage decreases with radial distance (nondimensionalized to multiples of cavern radii) into the salt, away of the cavern, as shown in Figure 9, at different times. Interestingly, the calculated damage is quite small, even though all the conditions of material and stress were selected to produce the maximum damage possible. For example, if clean salt properties were used rather than the 3.0% impurity properties, virtually no damage would be calculated. As Munson et al. [1998] indicated, the results suggest that cylindrical caverns are resistant to development of damage, and hence fracture, because of their favorable configuration. Stresses around the cavern are largely compressive. Creep closure occurs of course, but the stress condition around the cavern is one that largely suppresses damage formation. Under these conditions of a smooth walled, cylindrical cavern, the results suggest that the maximum damage always is at the cavern wall. Fracture, if it occurs, probably results only in the gradual loss of material from the walls. Accumulation of material on the floor with time in excess of that thought to be the result of salt falls may be from this cause.

Other consequences of damage around the cavern are relatively clear. Although the damage extends into the salt, the microcracks that form, even if they are connected, cannot increase storage volume. Creation of the microcracks in depth in the salt merely causes the cavern wall to move inward slightly so that the salt mass is conserved. Even if the microcracks are connected to produce a local increase in permeability, permeation of the cavern fluid into the adjacent salt is not possible, because the far field impermeable salt still prevents loss from the cavern volume. Only if the far field salt has measurable permeability is permeation away from the cavern possible.

DISCUSSION AND SUMMARY

For a number of potential applications of older caverns, it will be necessary to understanding in more detail the fracture and failure of salt. In fact, fracture has been approached scientifically through many diverse concepts. Here, a specific model of fracture has been developed for salt, which uses the concept of continuum damage. When combined with a transient and steady state model of creep, the constitutive model treats all aspects of the time-dependent behavior, including tertiary creep and failure. Healing of damage is also treated as a rate-dependent process. The guide for model development is the dislocation mechanism map and the fracture mechanism map for salt. These maps restrict the number of possible mechanisms and mechanisms appropriately suggest some independently determined physical constants. The model utilizes the formation and evolution of microfractures under the prevailing stress conditions to describe the fracture process. The Multimechanism Deformation Coupled Fracture (MDCF) constitutive model is the result of this development and it represents quite accurately the creep data upon which it is based. In addition, the application of the model to numerical simulations of large-scale field experiments has provided substantial verification. With a relatively sophisticated constitutive model, validated through independent simulation of field tests, one has some assurance of the predictive capability of the analysis system.

The model and analysis system was used to determine the expected behavior of a cylindrical cavern in salt. While damage is generated around the cavern, it is not as pronounced as might be expected. Damage is a function of the depth in the cavern, and is maximum at the bottom of the cavern. The amount of damage also depends upon the impurity content of the salt, with impure salt more susceptible to damage. Because the damage is essentially restricted to the salt adjacent to the cavern, fluid loss or permeation into the salt is probably not possible unless the salt has a measurable far field permeability.

REFERENCES

Ashby, M.F., 1983. Mechanisms of Deformation and Fracture, Advances in Applied Mechanics, **23**, 117-177.

Aubertin, M., J. Sgaoula, and D.E. Gill, 1993. A Damage Model for Rocksalt: Application to Tertiary Creep, 7th Sym. on Salt, eds., H.Kakihana, H.R. Hardy, Jr., T. Hoshi, and K. Toyokura, Elsevier Science Publications, NY, **1**, 511-523.

Aubertin, M., J. Sgaoula, S. Servant, M.R. Julien, D.E. Gill, and B. Landanyi, 1998. An Up-to-Date Version of SUVIC-D for Modeling the Behavior of Salt, Proc. 4th Conf. on the Mech. Behavior of Salt, Trans Tech Publications, Clausthal-Zellerfeld, Germany, 205-220.

Borns, D.J., and J.C. Stormont, 1989. The Delineation of the Disturbed Rock zone Surrounding Excavations in Salt, Proc. 30th U.S. Symp. on Rock Mech., A.A. Balkema, Rotterdam, Netherlands, 353-360.

Brodsky, N.S., and D.E. Munson, 1994. Thermomechanical Damage Recovery Parameters for Rocksalt from the Waste Isolation Pilot Plant, Proc. 1st N. Am. Rock Mech. Symp., eds. P.P. Nelson and S.E. Lauback, A.A. Balkema, Rotterdam, Netherlands, 731-738.

Chan, K.S., S.R. Bodner, A.F. Fossum, and D.E. Munson, 1992. A Constitutive Model for Inelastic Flow and Damage Evolution in Solids under Triaxial Compression, Mech. of Mat., **14**,1-14.

Chan, K.S., N.S. Brodsky, A.F. Fossum, S.R. Bodner, and D.E. Munson, 1994. Damage-Induced Nonassociated Inelastic Flow in Rock Salt, Int'l J. of Plasticity, **10**, 623-642.

Chan, K.S., S.R. Bodner, A.F. Fossum, and D.E. Munson, 1995a. Constitutive Representation of Damage Healing in WIPP Salt, 35th U.S. Symp. on Rock Mech., A.A. Balkema, Rotterdam, Netherlands, 485-490.

Chan, K.S., K.L. DeVries, S.R. Bodner, A.F. Fossum, and D.E. Munson, 1995b. A Damage Mechanics Approach to Life Prediction for a Salt Structure, Computational Mechanics '95, eds. S.N. Alturi, G. Yagawa, and T.A. Cruse, Vol. 1, 1140-1145.

Chan, K.S., D.E. Munson, A.F. Fossum, and S.R. Bodner, 1996a. Inelastic Flow Behavior of Argillaceous Salt, Int'l J. Damage Mech., **5**, 292-314.

Chan, K.S., D.E. Munson, A.F. Fossum, and S.R.Bodner, 1996b. Cleavage and Creep Fracture of Rock Salt, Acta Materialia, **44**, 3553-3565.

Chan, K.S., S.R. Bodner, A.F. Fossum, and D.E. Munson, 1997a. A Damage Mechanics Treatment of Creep Failure in Rock Salt, Int'l J. Damage Mech., **6**, 121-152.

Chan, K.S., N.S. Brodsky, A.F. Fossum, D.E. Munson, and S.R. Bodner, 1997b. Creep Induced Cleavage Fracture in WIPP Salt under Indirect Tension, J. Eng. Mat. Tech., **119**, 393-400.

Chan, K.S., D.E. Munson, A.F. Fossum, and S.R. Bodner, 1998a. A Constitutive Model for Representing Coupled Creep, Fracture, and Healing in Rock Salt, Proc. 4th Conf. on the Mech. Behavior of Salt, Trans Tech Publications, Clausthal-Zellerfeld, Germany, 221-234.

Chan, K.S., S.R. Bodner, and D.E. Munson, 1998b. Recovery and Healing of Damage in WIPP Salt, Int'l J. Damage Mech., **7**, 143-166.

Cristescu, N., 1993. A General Constitutive Equation for Transient and Stationary Creep of Rock Salt, Int'l J. Rock Mech. Min. Science & Geomech. Abstr., **30**, 125-140.

Desai, C.S., and D. Zhang, 1987. Viscoplastic Model for Geologic Materials with Generalized Flow Rule, Int'l J. Numerical and Analytic Methods in Geomech., **11**, 603-620.

Fossum, A.F., Callahan, G.D., L.L. Van Sambeek, and P. Senseny, 1988. How Should One-Dimensional Laboratory Equations be Cast into Three-Dimensional Form?, Proc. 29th Symp. on Rock Mech., A.A. Balkema, Rotterdam, Netherlands, 35-41.

Fossum, A.F., N.S. Brodsky, K.S. Chan, and D.E. Munson, 1993. Experimental Evaluation of a Constitutive Model for Inelastic Flow and Damage Evolution in Solids Subjected to Triaxial Compression, Int'l J. Rock Mech. Min. Science & Geomech. Abstr., **30** 1341-1344.

Hayhurst, D.R., 1972. Creep Rupture under Multi-Axial States of Creep, J. Mech. Physics Solids, **20**, 381-390.

Kachanov, L.M., 1958. On Creep Rupture Time, Otdelenie Teknicheskikh Nauk, Izvestiya Akademii Nauk SSSR, **8**, 26-31.

Krajcinovic, D., 1984. Continuum Damage Mechanics, Appl. Mech. Rev., **37**, 1-6.

Lux, K-H., A. Hou, and U. Dusterloh, 1998. Some New Aspect in Modelling of Salt Cavern Behaviour and Safety Analysis, Proc. Solution Mining Research Institute Fall Meeting 1998, Rome, Italy, SMRI, Deerfield, IL, 361-389.

Munson, D.E., 1979. Preliminary Deformation Mechanism-Map for Salt (with Application to WIPP), SAND79-0076, Sandia National Laboratories, Albuqueque, NM.

Munson, D.E., and P.R. Dawson, 1984. Salt Constitutive Modeling using Mechanism Maps, Proc. 1st Conf. on the Mech. Behavior of Salt, Trans Tech Publications, Clausthal-Zellerfeld, Germany, 717-737.

Munson, D.E., A.F. Fossum, and P.E. Senseny, 1989. Advances in Resolution of Discrepancies between Predicted and Measured In-Situ WIPP Room Closures, SAND88-2948, Sandia National Laboratories, Albuquerque, NM.

Munson, D.E., and W.R. Wawersik, 1991. Constitutive Modeling of Salt Behavior – State of the Technology, 7th Int'l Congress on Rock Mech., ed. W. Wittke, A.A. Balkema, Rotterdam, Netherlands, 1797-1810.

Munson, D.E., D.J. Holcomb, K.L. DeVries, N.S. Brodsky, and K.S. Chan, 1995. Correlation of Theoretical Calculations and Experimental Measurements of Damage around a Shaft in Salt, Proc. 35th U.S. Symp. on Rock Mech., A.A. Balkema, Rotterdam, Netherlands, 491-496.

Munson, D.E., A.L. Jensen, S.W. Webb, and K.L. DeVries, 1996. Brine Release Based on Structural Calculations of Damage Around an Excavation at the Waste Isolation Pilot Plant (WIPP), Proc. 2nd N. Am. Rock Mech. Symp., A.A. Balkema, Rotterdam, Netherlands, 1495-1500.

Munson, D.E., 1997. Constitutive Model of Creep in Rock Salt Applied to Underground Room Closure, Int'' J. Rock Mech. Min. Sci. & Geomech. Abstr., **34**, 233-247.

Munson, D.E., M.A. Molecke, and R.E. Myers, 1998. Interior Cavern Conditions and Salt Fall Potential, Proc. Solution Mining Research Institute Spring Meeting 1998, El Paso, TX, SMRI, Deerfield, IL, 226-239.

Schulz, R., H. Denzau, and K. Benke, 1998. Introduction of a Continuum Damage Method (CDM) for FEM Calculations of Fracture Mechanisms in Salt, Proc. Solution Mining Research Institute Fall Meeting 1998, Rome, Italy, SMRI, Deerfield, IL, 489-502.

Stormont, J.C., J.J.K. Daemen, and C.S. Desai, 1992. Prediction of Dilation and Permeability Changes in Rock Salt, Int'l J. Numerical and Analytic Methods in Geomech., **16**, 545-569.

Webb, S.W., 1992. Brine Inflow Sensitivity Study for Waste Isolation Pilot Plant Boreholes: Results of One-Dimensional Simulations, SAND91-2296, Sandia National Laboratories, Albuquerque, NM.